

595-90

~ 140950  
 N93-19208

The spatial distribution of large cometary meteoroids in the inner solar system

Neil McBride & David W. Hughes. Department of Physics, University of Sheffield, Sheffield, S3 7RH, UK.

**Abstract.** A model for the spatial density distribution of large ( $m > 10^{-3}$  g) cometary meteoroids in the inner solar system is obtained assuming that they have orbits closely associated with that of their parent comet. Distributions of the orbital parameters of the Taurid, Quadrantid and Perseid meteoroid streams are used in developing the model.

**Introduction**

Hughes & McBride (1990) used the group of 135 known short-period comets as listed by Marsden (1986), and placed meteoroids on each orbit. This effectively turned each orbit into a thin meteoroid stream. The relative spatial density distribution of the cometary meteoroids was then obtained. The semi-major axis distribution of the Quadrantid meteoroid stream was incorporated to improve the model.

In this paper, each short-period comet orbit is replaced by a suite of 175 new orbits, the orbital characteristics of which reflect a 'typical' meteoroid stream. 1000 equal mass particles are then put on each of the 23,625 orbits such that the mass flow ( $\text{g s}^{-1}$ ) is constant. The particles are assumed to be large ( $m > 10^{-3}$  g) such that they can be taken to be in stream closely associated with their parent comet. The relative spatial density distribution of all the particles is then obtained.

**Modelling a meteoroid stream**

Fig. 1 shows histograms of the semi-major axis distributions of Taurid, Quadrantid and Perseid meteoroids. The 57 Quadrantid meteor orbits were measured by the Radio Meteor Project (see Sekanina, 1970), the 178 Taurid (67 Northern and 111 Southern) and the 12 Perseid meteor

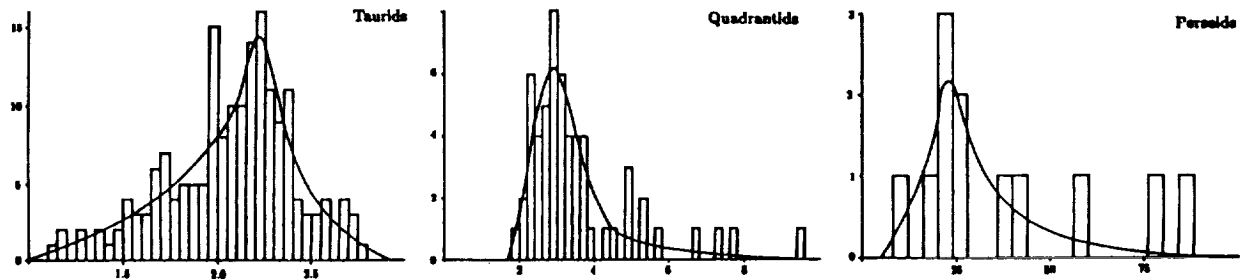


Figure 1. The semi-major axis distributions. The abscissae are in AU.

orbits were obtained from the meteor data base held at the International Meteor Data Centre, University of Lund, Sweden. For this simple model, cosmic weightings have not been applied as the variation in velocity within each given stream is relatively small. Smooth curves were

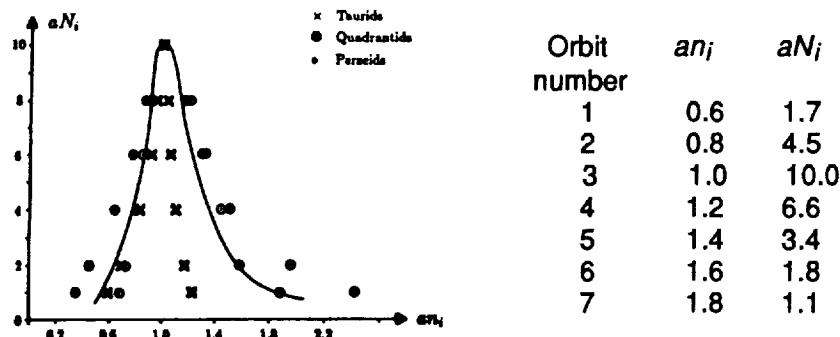


Figure 2. The standardised semi-major axis distributions for the three streams. The solid curve shows the mean distribution. The table shows the parameters used to model semi-major axis.

fitted to the histograms such that the areas under each histogram and its fitted curve is equal. The peak of each curve has an ordinate of  $N_p$  and an abscissa of  $x_p$ . Points were recorded from each curve, each point having an ordinate  $N$  and an abscissa  $x$ . These points were then replotted on the graph shown in Fig. 2. Here the ordinate is ten times the ratio  $N/N_p$  and is labelled  $aN_i$ . The abscissa gives the ratio  $x/x_p$  and is labelled  $an_i$ .

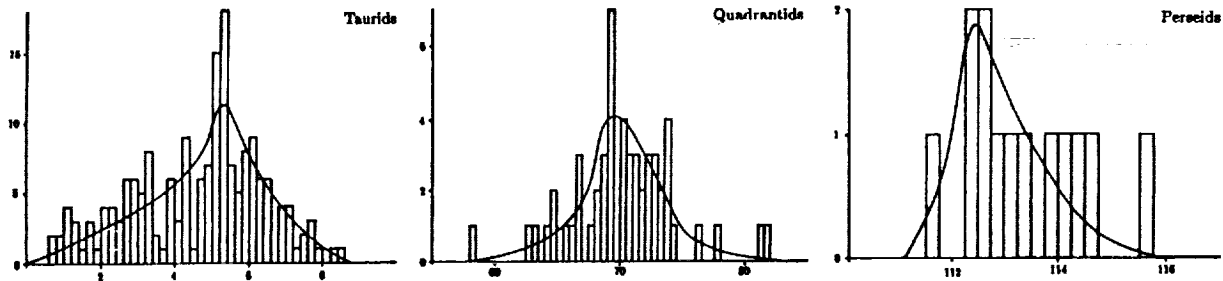


Figure 3. The inclination distributions. The abscissae are in degrees.

By doing this, the three distributions shown in Fig. 1 have been 'standardised', and are easily inter-compared. To obtain a 'typical' semi-major axis distribution, a curve was fitted such that any point on the curve represents the mean of the three stream distributions. Seven points were then read off this curve, having ordinates  $aN_i$  and abscissae  $an_i$  ( $i=1$  to 7). These are given in the table in Fig. 2. Any comet orbit with semi-major axis  $a$  can then be replaced with 7 orbits each with semi-major axis  $an_i \times a$ . The modelling is completed by scaling the number of particles on each orbit by the factor  $aN_i$ .

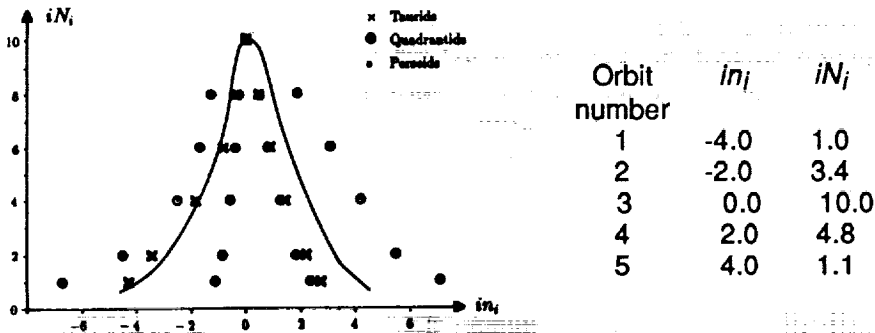


Figure 4. The standardised inclination distributions for the three streams. The solid curve shows the mean distribution. The table shows the parameters used to model inclination.

The orbital inclination  $i$  is modelled in a similar fashion. Fig. 3 shows histograms of the inclination distribution for 3 streams, and Fig. 4 shows the standardised distributions. The ordinate in Fig. 4 is now labelled  $iN_i$  and the abscissa  $in_i$ . Note that the abscissae are now given by  $x-x_p$ . Points from the mean distribution give the values shown in the table. Any comet orbit with inclination  $i$ , can be replaced with 5 orbits each with inclination  $i+in_i$ . The number of meteoroids placed on each orbit is scaled by the factor  $iN_i$ .

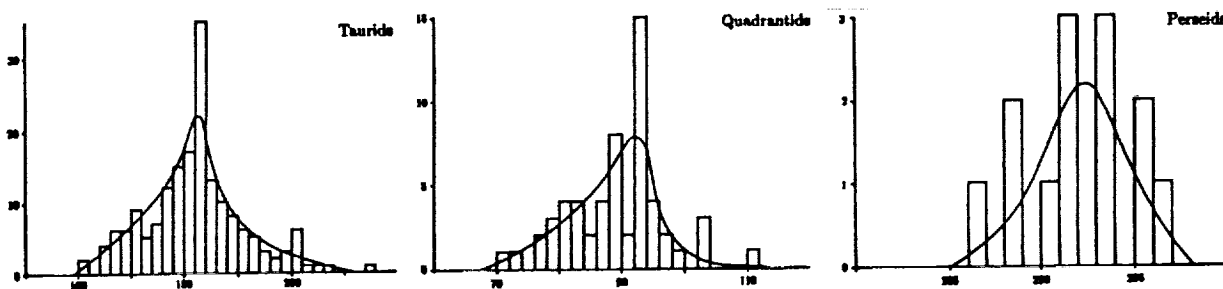


Figure 5. The longitude of perihelion distributions. The abscissae are in degrees.

Finally, the longitude of perihelion  $L$  (defined here as  $\omega + \Omega$ ) is modelled in the same way as the inclination. Fig. 5 shows histograms of  $L$  for the 3 streams. The standardised distribution is shown by the graph in Fig. 6, where the ordinate is labelled  $LN_i$  and the abscissa is labelled  $Ln_i$ . The table gives the scaling factors such that a comet orbit with longitude of perihelion  $L$  can be replaced with 5 orbits each with longitude of perihelion  $L + Ln_i$ . The number of particles on each orbit are scaled by the factor  $LN_i$ . It is seen then that by taking a comet orbit and generating new orbital parameters as described above (in a 'nested loop' fashion), 175 orbits are produced.

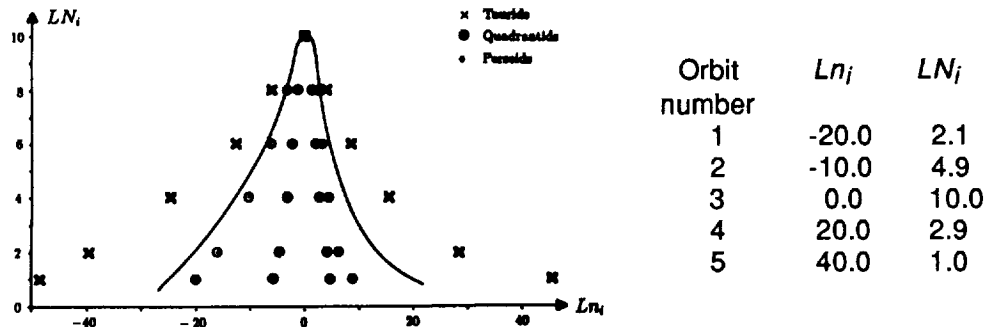


Figure 6. The standardised longitude of perihelion distributions for the three streams. The solid curve shows mean distribution. The table shows the parameters used to model longitude of perihelion.

#### Modelling the spatial density distribution of cometary meteoroids

Each of the 135 short-period comet orbits were replaced by 175 generated orbits, the orbital parameters of which depending on the orbital parameters of the parent comet, as described above. 1000 particles were put on each orbit, this number being scaled by the factors  $an_i$ ,  $in_i$  and  $Ln_i$ . A  $z$  and  $R$  co-ordinate system was used where

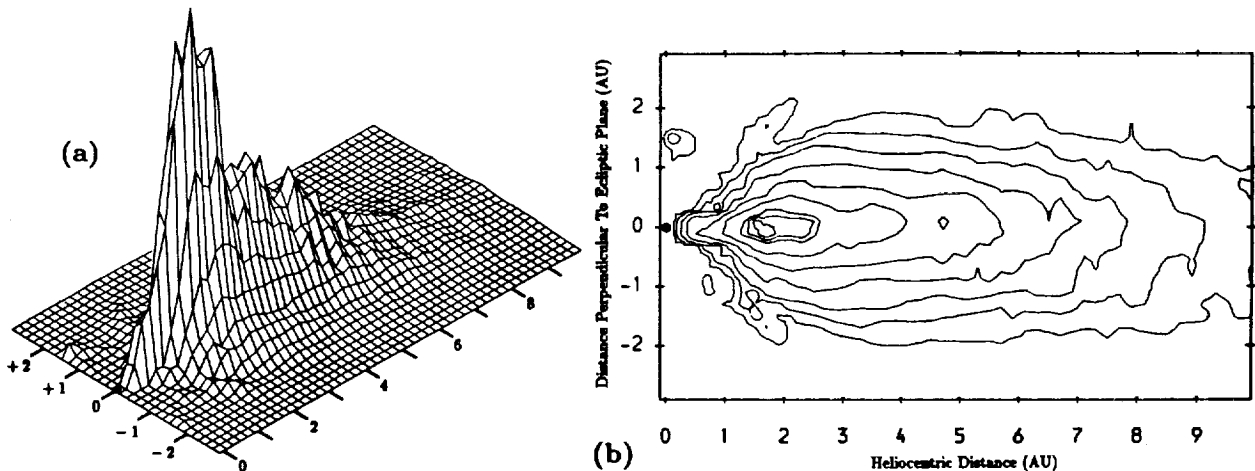


Figure 7. (a) The height represents the spatial density. The ground level corresponds to the  $z$ - $R$  plane with  $0 < R < 10$  AU and  $-3 < z < +3$  AU. The black dot represents the Sun. (b) A contour plot of Fig. (a). The abscissa is the distance  $R$  and the ordinate is the distance  $z$ . The spatial density is in arbitrary units, the contours representing 10, 25, 50, 100, 200, 400, 760, 890 and 1020 these units.

$R$  is defined as the meteoroid heliocentric distance projected into the ecliptic, and  $z$  is the distance perpendicular to the ecliptic. The particles can then be binned into grid squares in this  $z$ - $R$  plane. A grid square in this plane represents the volume of space swept out by revolving the square around an axis which is perpendicular to the ecliptic and passes through the Sun. The spatial density was found by dividing the number of particles binned in the square by this volume. This spatial density distribution in the  $z$ - $R$  plane is shown in Fig. 7. The ecliptic spatial density is shown in Fig. 8, this being the spatial density of the particles with  $-2.0 < z < +2.0$  AU.

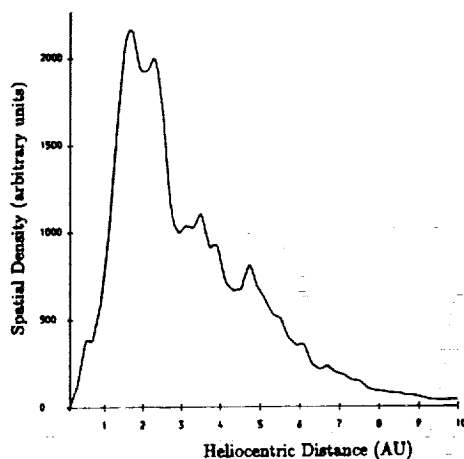


Figure 8. The spatial density of the stream meteoroids in the ecliptic ( $-0.2 < z < +0.2$  AU) is plotted as a function of heliocentric distance.

It can be seen from Figs. 7 and 8 that the distribution of large cometary meteoroids has a torus-like shape, centred on the Sun. The central hole extends to about 0.5 AU, and the outer edge is around 6 AU. It can be seen that the spatial density varies in a rather complicated way as a function of the ecliptic heliocentric distance. Note that the density at 1 AU is not typical. In the meteoroid particle size range under consideration there is a considerable increase in the spatial density as one moves out from the Sun to an ecliptic heliocentric distance of about 1.7 AU. The density near the 1.7 AU peak is around four times the 1.0 AU value. The relative spatial densities at the orbits of the Earth, Mars, Jupiter and Saturn are in the ratios 1.0 : 2.5 : 0.7 : 0.1. It is only beyond about 2.5 AU that the density starts to decrease dramatically and space becomes less hazardous for planetary probes and the surfaces of cometary nuclei. The profile in Fig. 8 does not appear to follow any simplified power law relationship, although there may be some justification for arguing a power law fall-off at distances greater than about 2 AU. At this distance ( $2 < R < 10$  AU) the drop-off crudely follows a  $R^{-2.2}$  relationship.

It must be stressed that these results can only really be applied to large particles; relatively young meteoroids that have not been significantly affected by the Poynting-Robertson effect. These meteoroids are much larger than the dust particles responsible for the Zodiacal Cloud. This torus of cometary meteoroids will however act as a mass reservoir from which the Zodiacal Cloud can be maintained (by fragmentation due to impacts and erosion). It should be pointed out that the central hole of the torus will be occupied by these smaller dust decay products.

### References

- Hughes, D.W. & McBride, N., 1990. *Mon. Not. R. astr. Soc.*, **243**, 312.  
 Marsden, B.G., 1986. *Catalogue of Cometary orbits*, 5th edn, International Astronomical Union.  
 Sekanina, Z., 1970. *Icarus*, **13**, 459.